Applied Physics Letters

Identification of the defect dominating high temperature reverse leakage current in vertical GaN power diodes through deep level transient spectroscopy

Cite as: Appl. Phys. Lett. **120**, 053502 (2022); https://doi.org/10.1063/5.0082257
Submitted: 13 December 2021 • Accepted: 12 January 2022 • Published Online: 31 January 2022

S. DasGupta, O. Slobodyan, T. Smith, et al.

Applied Physics Letters ARTICLE scitation.org/journal/apl

Identification of the defect dominating high temperature reverse leakage current in vertical GaN power diodes through deep level transient spectroscopy

Cite as: Appl. Phys. Lett. **120**, 053502 (2022); doi: 10.1063/5.0082257
Submitted: 13 December 2021 · Accepted: 12 January 2022 ·
Published Online: 31 January 2022

S. DasGupta,[a] O. Slobodyan, T. Smith, A. Binder, J. Flicker, R. Kaplar, J. Mueller, L. Garcia Rodriguez, and S. Atcitty

AFFILIATIONS

Sandia National Laboratories, Albuquerque, New Mexico 87185, USA

Note: This paper is part of the APL Special Collection on Wide- and Ultrawide-Bandgap Electronic Semiconductor Devices.
[a]**Author to whom correspondence should be addressed:** sdasgup@sandia.gov

ABSTRACT

Deep level defects in wide bandgap semiconductors, whose response times are in the range of power converter switching times, can have a significant effect on converter efficiency. We use deep level transient spectroscopy (DLTS) to evaluate such defect levels in the n-drift layer of vertical gallium nitride (v-GaN) power diodes with $V_{BD} \sim 1500$ V. DLTS reveals three energy levels that are at ~0.6 eV (highest density), ~0.27 eV (lowest density), and ~45 meV (a dopant level) from the conduction band. Dopant extraction from capacitance–voltage measurement tests (C–V) at multiple temperatures enables trap density evaluation, and the ~0.6 eV trap has a density of 1.2×10^{15} cm^{-3}. The 0.6 eV energy level and its density are similar to a defect that is known to cause current collapse in GaN based surface conducting devices (like high electron mobility transistors). Analysis of reverse bias currents over temperature in the v-GaN diodes indicates a predominant role of the same defect in determining reverse leakage current at high temperatures, reducing switching efficiency.

Solid-state devices are the most crucial components of power electronic systems, which facilitate conversion of electrical power from the generation source into a form suitable for consumption by electrical loads for various applications. Silicon devices have dominated the field of power electronics due to having moderately suitable thermal properties and a very high level of maturity with respect to process, reliability, and cost considerations. Wide-bandgap (WBG) semiconductors like gallium nitride (GaN), silicon carbide, or diamond have intrinsic properties that are much more suitable for high power applications (such as higher critical electric field and thermal conductivity).[1–11] The performance and reliability of lateral WBG devices like GaN high electron mobility transistors (HEMTs) have fallen short of their potential because GaN layers grown on mismatched, non-native substrates (Si, SiC, or sapphire) inhibit the realization of vertical device structures due to high defect densities ($>10^8$–10^9 cm^{-2}), as well as the difficulty of field engineering in lateral 2D electron gas (2DEG) based GaN devices.

Low defect density is important for power devices because it affects multiple performance characteristics (e.g., breakdown voltage and OFF-state leakage current), yield, reliability (stability under stress at high temperature, reverse bias, or forward current, operating life, avalanche ruggedness), and cost. In other technologies, such as optical devices, GaN/InGaN lasers have shown notable improvement in defect density using native bulk GaN substrates.[12,13]

It is generally understood that lateral device architectures (that are more developed with epitaxial GaN on Si) are less suited to power applications due to the prohibitively high thermal energy densities required. Vertical structures are optimal for achieving higher breakdown voltage (V_{BD}) and large currents as are usually required in utility scale power conversion. Therefore, the development of GaN substrates and epitaxial layers with low densities of electrically active defects remains key to realizing the potential of the wide bandgap material as a much higher efficiency alternative to silicon in the area of power conversion.

In this study, we use deep level transient spectroscopy (DLTS)[14] to evaluate defects whose response times are ~10 ms or less. Since power converters usually operate in the ~10 to ~100 kHz frequency range depending on the power levels being handled, this is the range of response times where defects can have an effect on converter

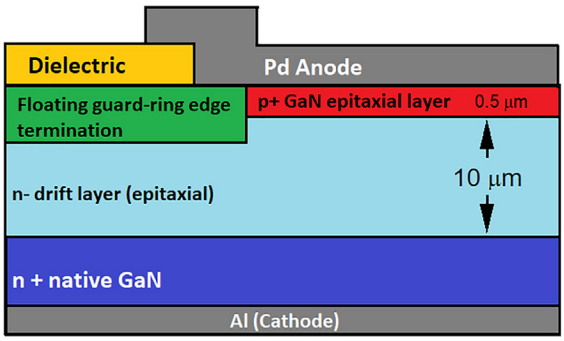

FIG. 1. Schematic of a vertical GaN (v-GaN) p–n diode on native GaN substrate.

efficiency. DLTS reveals three energy levels that are at ∼0.6 eV (highest density), ∼0.27 eV (lowest density), and ∼45 meV (a dopant level) from the conduction band. Dopant extraction from C–V at multiple temperatures enables trap density evaluation. The ∼0.6 eV trap has a density of $1.2 \times 10^{15}\,\mathrm{cm}^{-3}$. The ∼0.6 eV energy level and its density are similar to a defect that is known to cause current collapse in GaN based surface conducting devices (like HEMTs). Analysis of reverse bias currents over temperature in the vertical GaN (v-GaN) diodes indicates a predominant role of the same defect in determining reverse leakage at high temperatures, reducing switching efficiency.

The devices used in the study (Fig. 1) were grown by low-pressure metal organic chemical vapor deposition (MOCVD) on pseudo-bulk GaN substrates grown by hydride vapor phase epitaxy (HPVE) with a low threading dislocation density (TDD) of 10^4–$10^6\,\mathrm{cm}^{-2}$. 0.5 μm p^+ layers are doped with Mg at a concentration $2 \times 10^{19}\,\mathrm{cm}^{-3}$, and a higher level of doping was used at the surface layer for low contact resistance.[15–17]

The net doping ($N_d - N_a$) of the n-drift layer is the most important factor controlling the depletion depth and electric field in reverse bias. For kV-level operation, net doping level in the n-drift layer has to be in the range of 10^{15}–$10^{16}\,\mathrm{cm}^{-3}$.

The capacitance transient DLTS method, which has been extensively discussed and utilized for characterizing deep level defects, was used to characterize electrically active defects in the *n*-drift layer. The devices were operated at a reverse bias of −9 V. Since the widths on the *p*+ and *n*− sides of the *p*–*n* junction are inversely related to the doping on the two sides, the reverse bias creates a depletion region almost exclusively on the *n*− side. A fill pulse of 0 V is used to populate traps in the drift region, and the capacitance transient is measured at a reverse bias of −9 V with a 100 kHz small signal frequency (from traps depopulating through thermal emission of electrons). Figure 2 shows raw DLTS capacitance delta transients in (a) linear and (b) log scales over a temperature range of 15–400 K. Temperature scans with boxcar sampling over five different rate windows (200, 500, 1000, 2000, and 5000 s^{-1}) (*T1* through *T5* in Fig. 2) are used to generate the Arrhenius analysis, which reveals the important trap parameters, where the energy level for the defect responsible for a given set of emission peaks is obtained from the slope of $\ln(\tau T^2)$ vs T^{-1} (T being the temperature peak and τ being the inverse of the rate window),

$$E_a = \frac{d[\ln(\tau T^2)]}{d[1/k_B T]}, \tag{1}$$

and the cross section (electron emission cross section in this case) is obtained from the intercept of the same,

$$\sigma = \frac{e^{-intercept}}{\gamma_n}, \tag{2}$$

where $\gamma_n = 2\,(3k_B/m_n)^{1/2}\,(2\pi m_n k_B/h^2)^{3/2} = 3.25 \times 10^{21} \times m_e\,\mathrm{cm}^{-2}\,\mathrm{s}^{-1}\,\mathrm{K}^{-2}$, m_e being the effective electron mass for GaN.

Figure 2(c) shows Arrhenius plots with excellent linearity for the extracted peaks for the three defect energies: ∼0.6 eV (highest density), ∼0.27 eV (lowest density), and ∼45 meV (likely the dopant level) (Table I).

To calculate the trap densities, it is necessary to know the effective doping of the drift region, since the trap density is given by

$$N_T = 2rN_d\Delta C/C_0, \tag{3}$$

where r is a function of t_1 and t_2 (the two boxcar sampling times), given by

$$\mathrm{r} = \left[\exp\{\ln(t_1/t_2)/(t_2/t_1 - 1)\} - \exp\{\ln(t_1/t_2)/(1 - t_1/t_2)\}\right]^{-1}. \tag{4}$$

C_0 is the equilibrium capacitance and N_d is the effective doping of the drift region. To find the effective dopant density, we use the standard method of extraction from $1/C^2$ vs V slope in the reverse bias regime.[18] Figure 3(a) shows the $d(1/C^2)/dV$ slope over a temperature range of ∼−25 °C to 23 °C (room temperature) used to extract *n*-drift layer doping per the following equation:

$$N_d = \frac{2}{q\varepsilon}\left[\frac{d\left(A^2/C^2\right)}{dV}\right]^{-1}, \tag{5}$$

where ε is the permittivity of GaN, q is the electronic charge, and A is the device area = 0.72 mm^2. The method yields a value of $N_d = 8.8 \times 10^{15}\,\mathrm{cm}^{-3}$, which implies a trap density of $1.2 \times 10^{15}\,\mathrm{cm}^{-3}$ for the ∼0.6 eV energy level (*D1*) and a much lower density of $4 \times 10^{13}\,\mathrm{cm}^{-3}$ for the ∼0.27 eV energy level (*D3*).

For level *D2*, the peaks appear in the 20–30 K range. As Fig. 3(b) shows, at low temperature, starting from ∼30 to ∼20 K, the capacitance drops drastically to almost zero, indicating carrier freeze out dominating the *D2* DLTS peaks. Since the effective value of N_d changes throughout the range of *D2* peaks, Eq. (3) cannot be used to evaluate the density of *D2*. The low value of the activation energy and the carrier freeze out signature from the C–V characteristics are consistent with *D2* being the donor level, and its density is best extracted through Eq. (5).

A ∼0.6 eV trap has been detected consistently in AlGaN/GaN HEMTs by several groups employing a variety of different growth and passivation methods.[19–23] The ubiquitous nature of the trap regardless of the nature of the barrier layer in the HEMT heterostructures has led some researchers to speculate that the defect belongs to the epitaxially grown GaN, rather than to a specific barrier or passivation layer material. More recently, MOCVD grown GaN on native substrates has demonstrated the ∼0.6 eV trap (and also the ∼0.27 eV trap) and has been correlated with Fe contamination, with the wafer cleaning process and wafer susceptor being identified as the sources. The trap is also shown to have an inverse correlation with C impurity levels.[24,25]

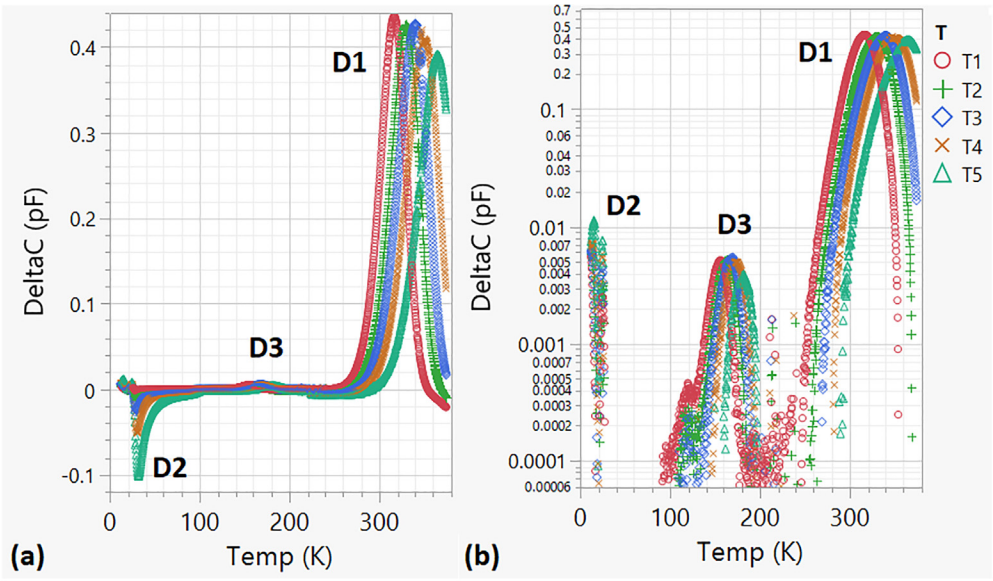

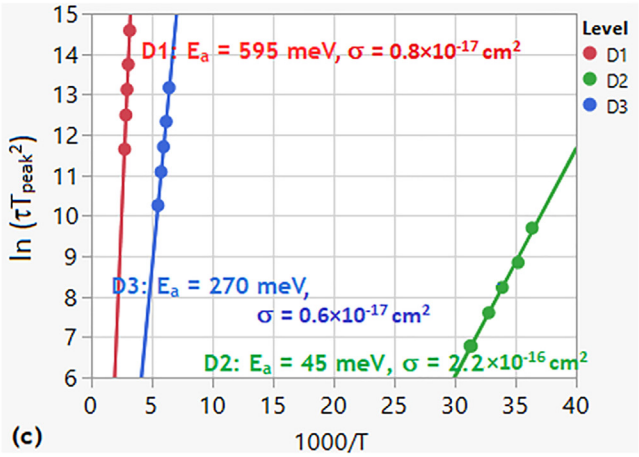

FIG. 2. Raw DLTS capacitance delta transients in (a) linear and (b) log scales over a temperature range of 15–400 K. A fill pulse of 0 V is used to populate traps in the lightly doped n^- drift region, and the capacitance transient is measured at a reverse bias of −9 V, 100 kHz small signal frequency. Three peaks, *D1*, *D2*, and *D3* are visible. (c) Arrhenius plots for the extracted peaks demonstrate three defect energies: ∼0.6 eV (highest density), ∼0.27 meV (lowest density), and ∼45 meV (most likely a dopant level).

The significance of the *D1* energy level in device operation in a power converter is understood by analyzing the reverse bias leakage over a range of temperatures (323–423 K).

TABLE I. Summary of defect energies, cross sections, and densities for the defect peaks in Figs. 2(a) and 2(b).

Level	T_{peak}@ 2000 s^{-1} RW	*Ea* (meV)	σ (cm^2)	N_T (cm^{-3})
D1	351 K	593	0.8×10^{-17}	1.2×10^{15}
D2	30.5 K	47.9	2.2×10^{-16}	⋯
D3	173 K	268.7	0.6×10^{-17}	4×10^{13}

Figure 4 shows the reverse bias current in a v-GaN diode over a temperature range of 323–423 K (−5 to −1400 V). At the lower voltages (and hence lower currents), the data are noisy, but in the higher voltage range (−800 to −1400 V), it is possible to do an Arrhenius analysis [Fig. 5(a)]. The plot for ln|*I*| vs 1000/*T* shows good linearity. At higher voltages [Fig. 5(b)], the extracted activation barrier is low, but increases as the voltage is reduced. For reverse biases below 1000 V, the activation barrier increase flattens out and approaches ∼0.6 eV, which is extremely close to the *D1* activation energy.

The similarity between the *D1* activation energy and the activation barrier extracted from high temperature *I*–*V* provides insight into the conduction mechanism under reverse bias at high temperatures. For semiconductors with lower bandgaps (e.g., silicon), the reverse bias regime could be dominated by Shockley–Read–Hall (SRH)

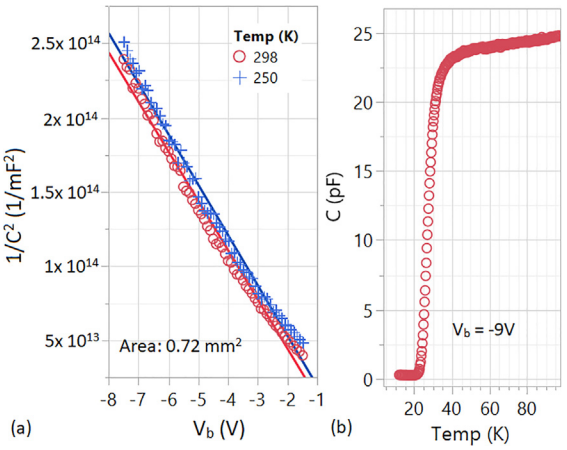

FIG. 3. (a) d(1/C^2)/dV slope over a temperature range of ∼ −23 °C to 25 °C (room temperature) used to extract the n-drift layer doping per Eq. (5). $N_d = 8.8 \times 10^{15}$ cm^{-3}. (b) At low temperature, starting from ∼30 to ∼20 K, the capacitance drops drastically to almost zero, indicating carrier freeze out dominating the *D2* DLTS peaks.

generation. If the reverse current in v-GaN diodes were dominated by SRH generation, one could have expected (i) minimal dependence on voltage or field on the extracted activation barrier, and (ii) an activation barrier representative of the defect's energy difference from the valence band, since the larger energy difference would make hole emission the rate limiting process (assuming similar emission cross sections for electrons and holes). We observe that neither of the above two criteria are satisfied by the reverse leakage characteristics, which is not surprising considering the very low intrinsic carrier density of GaN (10^{-10} cm^{-3}), which might cause mechanisms different from SRH to dominate the reverse leakage.

The combination of field and temperature dependent elements of the effective activation barrier indicates an effect like Pool–Frenkel emission,[26] which usually dominates transport in insulators that also have very low intrinsic or trap assisted generation due to their wide bandgaps. In its simplest form (no electric field dependence of mobility and no diffusion based transport), the Pool–Frenkel current is given by

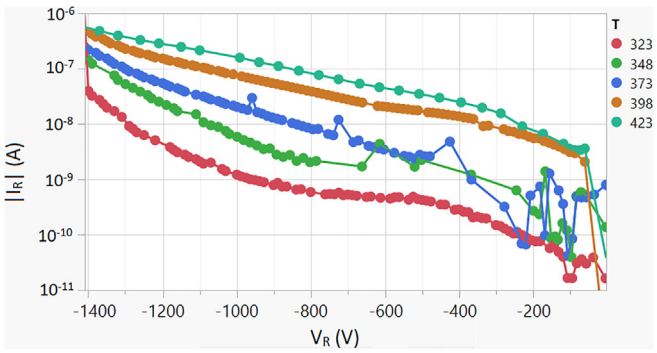

FIG. 4. Reverse bias current in a v-GaN diode over a temperature range of 323–423 K (−5 to −1400 V).

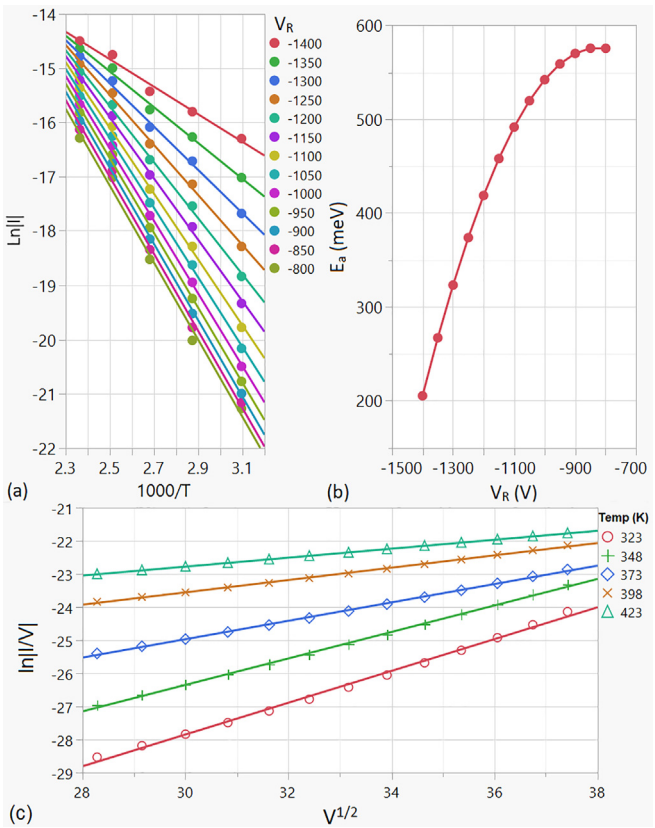

FIG. 5. (a) Arrhenius plots for reverse bias current in the −1400 to −800 V range. (b) At higher voltages, the activation barrier is low, but increases as voltage is reduced. For reverse biases below 1000 V, the activation barrier increase flattens out and closely approaches ∼0.6 eV. (c) The reverse bias current in the −1400 to −800 V shows the linear relationship between ln|I/V| and V$^{1/2}$ that characterizes Pool–Frenkel conduction.

$$J \propto E e^{\frac{-q\{\phi_b - (qE/\pi\varepsilon)^{1/2}\}}{k_B T}}, \tag{6}$$

where E is the electric field, T is the temperature, and ϕ_b is the thermal barrier for the emission of trapped electrons. At higher electric fields, the expectation would be one of increased barrier lowering, which we also observe [Fig. 5(b)]. The model described in Eq. (6) is ideal and according to it,

$$\partial(\ln|J|)/\partial(1/kT) = -q\{\phi_b - (qE/\pi\varepsilon)^{1/2}\}, \tag{7}$$

which means that ideally the slope of ln|J| vs 1/T at zero electric field should give the true barrier height in Pool–Frenkel conduction. Under such a scenario, the reverse current should exhibit continuous barrier lowering up to zero electric field. The analysis close to zero electric field is inhibited by the noisy currents at low voltages. It should also be noted that even drift based conduction should have mobility reduction at high electric fields, making the prefactor to the exponential term in Eq. (6) different from E. Also, at high electric field, the carrier temperature can be expected to deviate somewhat from the lattice temperature, introducing an electric field dependence of T itself, which means that

the conduction mechanism over the full reverse voltage range might deviate from an ideal Pool–Frenkel description. Regardless of what the exact model is, if any of the variations of Pool–Frenkel conduction (such as re-trapping, combined re-trapping and drift, hopping, or diffusion transport) were to represent the reverse bias conduction in the v-GaN diodes, at lower electric fields, one could expect the effective activation barrier to approach the actual thermal barrier (defect *D1* to conduction band energy ∼0.6 eV), which is indeed what Fig. 5(b) demonstrates. Also as Fig. 5(c) shows, the reverse bias current in the −1400 to −800 V exhibits the linear relationship between $\ln|I/V|$ and $V^{1/2}$ that characterizes Pool–Frenkel conduction. Thus, a combined analysis of the DLTS spectra and reverse currents over temperature in the v-GaN diodes indicates a predominant role of the ∼0.6 eV defect in determining reverse leakage current at high temperatures and high reverse voltage ranges, which could potentially reduce switching efficiency.

The results indicate the need for identifying the physical origins of the ∼0.6 eV defect and determining process vectors that can control the concentration of the defect during epitaxial growth to maximize the potential performance of v-GaN diodes in high power conversion.

Sandia National Laboratories is a multimission laboratory managed and operated by National Technology & Engineering Solutions of Sandia, LLC, a wholly owned subsidiary of Honeywell International Inc., for the U.S. Department of Energy's National Nuclear Security Administration under Contract No. DE-NA0003525. The work is funded by the DOE Office of Electricity Energy Storage Program managed by Dr. Imre Gyuk. This paper describes objective technical results and analysis. Any subjective views or opinions that might be expressed in the paper do not necessarily represent the views of the U.S. Department of Energy or the United States Government.

AUTHOR DECLARATIONS

Conflict of Interest

The authors have no conflicts of interest to disclose.

DATA AVAILABILITY

The data that support the findings of this study are available within the article.

REFERENCES

[1]H. Morkoc, S. Strite, G. B. Gao, M. E. Lin, B. Sverdlov, and M. Burns, J. Appl. Phys. **76**, 1363 (1994).
[2]B. J. Baliga, J. Appl. Phys. **53**, 1759 (1982).
[3]M. Bhatnagar and B. J. Baliga, IEEE Trans. Electron Devices **40**, 645 (1993).
[4]K. Shenai, R. S. Scott, and B. J. Baliga, IEEE Trans. Electron Devices **36**, 1811 (1989).
[5]U. K. Mishra, P. Parikh, and Y.-F. Wu, Proc. IEEE **90**, 1022 (2002).
[6]T. Kimoto, Jpn. J. Appl. Phys. **54**, 040103 (2015).
[7]T. Kachi, Jpn. J. Appl. Phys. **53**, 100210 (2014).
[8]H. A. Moghadam, S. Dimitrijev, J. Han, D. Haasmann, and A. Aminbeidokhti, IEEE Trans. Electron Devices **62**(8), 2670 (2015).
[9]P. Pande, S. Dimitrijev, D. Haasmann, H. A. Moghadam *et al.*, Solid-State Electron. **171**, 107874 (2020).
[10]M. Saremi, R. Hathwar, M. Dutta, F. A. M. Koeck, R. J. Nemanich, S. Chowdhury, and S. M. Goodnick, Appl. Phys. Lett. **111**, 043507 (2017).
[11]M. Saremi, "Modeling and simulation of the programmable metallization cells (PMCs) and diamond-based power devices," Ph.D. dissertation (Arizona State University, 2017).
[12]S. Nakamura, M. Senoh, S. Nagahama, N. Iwasa, T. Yamada, T. Matsushita, H. Kiyoku, Y. Sugimoto, T. Kozaki, and H. Umemoto, Jpn. J. Appl. Phys. **37**(3B), L309 (1998).
[13]S. Tomiya, T. Hino, S. Goto, M. Takeya, and M. Ikeda, IEEE J. Sel. Top. Quantum Electron. **10**, 1277 (2004).
[14]D. V. Lang, J. Appl. Phys. **45**, 3023 (1974).
[15]I. C. Kizilyalli, A. P. Edwards, O. Aktas, T. Prunty, and D. Bour, IEEE Trans. Electron Devices **62**, 414 (2015).
[16]I. C. Kizilyalli, A. P. Edwards, H. Nie, D. Bour, T. Prunty, and D. Disney, IEEE Electron Device Lett. **35**, 247 (2014).
[17]I. C. Kizilyalli, A. P. Edwards, H. Nie, D. Disney, and D. Bour, IEEE Trans. Electron Devices **60**, 3067 (2013).
[18]J. Hilibrand and R. D. Gold, RCA Rev. **21**, 245 (1960), see https://worldradiohistory.com/ARCHIVE-RCA/RCA-Review/RCA-Review-1960-Jun.pdf, pg. 97.
[19]A. R. Arehart, A. Sasikumar, G. Via, B. Winningham, B. Poling, E. Heller, and S. A. Ringel, in *2010 IEDM Technical Digest* (IEEE, 2010), p. 20.1.1.
[20]A. Sasikumar, A. Arehart, S. Kolluri, M. H. Wong, S. Keller, S. P. DenBaars, J. S. Speck, U. K. Mishra, and S. A. Ringel, IEEE Electron Device Lett. **33**, 658 (2012).
[21]J. Joh and J. del Alamo, IEEE Trans. Electron Devices **58**, 132 (2011).
[22]Y. Sin, B. Foran, J. Joh, and J. del Alamo, Phys. Status Solidi A **208**, 1611 (2011).
[23]A. Chini, V. di Lecce, M. Esposto, G. Meneghesso, and E. Zanoni, IEEE Electron Device Lett. **30**, 1021 (2009).
[24]T. Narita, M. Horita, K. Tomita, T. Kachi, and J. Suda, Jpn. J. Appl. Phys. **59**(10), 105505 (2020).
[25]Y. Zhang, Z. Chen, W. Li, H. Lee, M. R. Karim, A. R. Arehart, S. A. Ringel, S. Rajan, and H. Zhao, J. Appl. Phys. **127**, 215707 (2020).
[26]A. K. Jonscher, Thin Solid Films **1**(3), 213 (1967).